Front. Struct. Civ. Eng. 2022, 16(2): 239–249
https://doi.org/10.1007/s11709-021-0804-y

RESEARCH ARTICLE

Numerical analysis of vehicle-bridge coupling vibration concerning nonlinear stress-dependent damping

Pengfei LI[a,b], Jinquan ZHANG[a,b*], Shengqi MEI[b,c,d], Zhenhua DONG[a,b], Yan MAO[a,b]

[a] *Bridge and Tunnel Technology Research Center, Research Institute of Highway, Ministry of Transport, Beijing 100088, China*
[b] *National Engineering Laboratory of Bridge Structure Safety Technology, Research Institute of Highway, Ministry of Transport, Beijing 100088, China*
[c] *State Key Laboratory of Mechanical Behavior and System Safety of Traffic Engineering Structures, Shijiazhuang Tiedao University, Shijiazhuang 050043, China*
[d] *School of Civil Engineering, Shijiazhuang Tiedao University, Shijiazhuang 050043, China*
[*] *Corresponding author. E-mail: rioh_jqzhang@163.com*

ABSTRACT Damping is known to have a considerable influence on the dynamic behavior of bridges. The fixed damping ratios recommended in design codes do not necessarily represent the complicated damping characteristics of bridge structures. This study investigated the application of stress-dependent damping associated with vehicle-bridge coupling vibration and based on that investigation proposed the stress-dependent damping ratio. The results of the investigation show that the stress-dependent damping ratio is significantly different from the constant damping ratio (5%) defined in the standard specification. When vehicles travel at speeds of 30, 60, and 90, the damping ratios of the bridge model are 3.656%, 3.658%, and 3.671%, respectively. The peak accelerations using the regular damping ratio are 18.9%, 21.3%, and 14.5% of the stress-dependent damping ratio, respectively. When the vehicle load on the bridge is doubled, the peak acceleration of the mid-span node increases by 5.4 times, and the stress-related damping ratio increases by 2.1%. A corrugated steel-web bridge is being used as a case study, and the vibration response of the bridge is compared with the measured results. The acceleration response of the bridge which was calculated using the stress-dependent damping ratio is significantly closer to the measured acceleration response than that using the regular damping ratio.

KEYWORDS vehicle-bridge vibration system, dynamic analysis, stress-dependent damping, energy dissipation

1 Introduction

Vehicle loads and traffic-induced vibration result in bridge vibration, eventually decreasing the bridge's reliability and specifically their fatigue performance [1,2]. In addition, a bridge's vibration causes feedback, affecting traffic and reducing the comfort of vehicle occupants [3]. As a result, the control of vehicle-bridge coupling vibration has attracted the interest of researchers [4,5].

It is an indisputable fact that the use of different damping values can have a great influence on the results of structural dynamics analysis [6–8]. However, the damping effect has not been adequately addressed in bridge dynamics' analysis. In wind-resistant design specifications for highway bridges [9,10], the damping ratios of a steel bridge, a steel and concrete composite bridge, and a concrete bridge were set to 0.005, 0.01, and 0.02, respectively. Alipour et al. [11] suggested that in the seismic design specification of highway bridges in the Eurocode 8 [12] and Caltrans Seismic Design Criteria [13], the damping ratio of bridge structures should generally be 0.05 and that in special circumstances a correction coefficient could be used. Green [14] obtained the damping ratio of bridges in Ontario, Canada. The data collected indicated that the damping ratio ranged from 0.15% to 0.64% for a bridge span of less than 75 m and from 0.64% to 0.95% for a bridge span of more than 125 m. Billing [15] measured the damping ratio of 27 steel bridges, concrete bridges, and wood bridges in Ontario, Canada using traffic excitation tests; the results showed

Article history: Received Sep 22, 2021; Accepted Nov 22, 2021

that the damping ratio of the steel bridges and concrete bridges ranged from 0.4% to 0.7% and 0.8% to 3.8%, respectively. Li et al. [16] measured the damping ratios of 111 highway bridges under environment excitation and found that the damping ratios of simply supported bridges, continuous bridges, cable-stayed bridges, and suspension bridges were less than 3.5%, 6%, 2%, and 1.5%, respectively. In contrast, the damping ratio of the continuous rigid-frame bridges was between 0.5% and 2.5%. These results indicate that the damping ratios of bridges have been investigated on a large scale. Casas [17] believed that the damping ratio of bridges was correlated with the vibration amplitude, but the details of the relationship were not provided. Myrvoll et al. [18] measured the dynamic behavior of a cable-stayed bridge and determined that its damping ratio was less than 0.5%, which was far less than the design value. Magalhães et al. [19] used a free decay oscillation method and environmental vibration stimulation to obtain the damping ratio of three structures (stadium, pedestrian overpass, and cable-stayed bridge). The results of that simulation indicated that the environmental vibration stimulation method was easier to use, but it resulted in large differences in the results. If the average value of multiple measurements was used, the damping ratio was similar to that obtained by the free decay oscillation method. Rebelo et al. [20] adopted the same methods to investigate the dynamic behavior of six railway bridges with small and medium spans. The test results showed that the damping ratio obtained from the free decay oscillation method (> 5% in general) was much higher than that obtained from the environmental vibration stimulation method (about 2%). Ülker-Kaustell and Karoumi [21,22] proposed the following equation to describe the positive correlation between the damping ratio ξ and the acceleration a of composite railway bridges:

$$\xi = 0.006 + 0.104a. \tag{1}$$

Although Hart and Vasudevan [23] and Charney [24] reported a significant effect of the damping ratio on the structural response and proposed the correction coefficients, specific values of the damping ratio under different load conditions are not part of the different standards or specifications. Eyre and Tilly [25] and Tilly [26] conducted tests on 23 steel bridges and composite bridges with span lengths ranging from 17 to 213 m and observed a nonlinear relationship between the damping ratio and the vibration amplitude. In addition, the higher the vibration amplitude, the higher the damping ratio was. The main reason is that at low amplitude, material damping plays a dominant role, but at high amplitude, the node and base also have significant effects on the damping ratio. Green and Cebon [27] conducted dynamic tests on two highway bridges under an impact load. It was found that the measured damping ratios exhibited different trends for the two bridges, which was believed that it may have been caused by the magnitude of the excitation force.

Hou et al. [28] found that typical diseases have significant influence on the vehicle-induced dynamic response of CFST arch bridge. Sun [29] suggested that principal simple and sum combination resonance tongues are the most important resonance tongues. Therefore, damping measures are required to be applied on related modes. The vehicle-bridge effect in the Eurocode is empirically added some damping on the bridge, which seems to be unable to reveal the interaction of the vehicle-bridge system. Jin et al. [30] improved the accuracy of the adding damping model by deriving a semi-closed formula for this additional damping based on the principle of equivalent energy dissipation. Glatz and Fink [31] suggested that the additional damping for four European high-speed trains moving load model is non-conservative, and define a conservative additional damping functions depending on the natural bridge frequency, the bridge mass and the train type. Stoura and Dimitrakopoulos [32] proposed a multi-mode additional damping and found that additional damping can obtain negative values, which implies influx instead of dissipation of energy.

In recent years, the amplitude-dependent damping characteristics of structures have attracted increasing attention. Lazan [33] conducted numerous tests on damping of different materials, and it was found that damping was affected by the stress amplitude, the load history, and the temperature. The author found that it was challenging to generalize the effect of the load history and temperature on damping in a uniform equation; thus, the author established a relationship between damping and the stress of the material. The relationship between the energy dissipation per unit volume $\Delta U(\sigma)$ and the stress amplitude σ is expressed as follows:

$$\Delta U(\sigma) = J\sigma^n, \tag{2}$$

where J is the dissipation energy per unit volume of the material and n is the coefficient of the material and stress level.

The relationship between the energy dissipation per unit volume and the maximum stress amplitude is expressed as follows:

$$\Delta U(\sigma) = 6895(\sigma/\sigma_{\mathrm{f}})^{2.3} + 41360(\sigma/\sigma_{\mathrm{f}})^{8}, \tag{3}$$

where σ_{f} is the fatigue limit stress.

The stress-dependent dissipation factor η proposed by Lazan [33] represents the prototype of stress-dependent damping. The dissipation factor η is defined as the ratio of the dissipated vibration energy $\Delta U(\sigma)$ to the total vibration energy $U(\sigma)$:

$$\eta = \frac{1}{2\pi} \cdot \frac{\Delta U(\sigma)}{U(\sigma)}. \tag{4}$$

Stress-dependent damping can be calculated as viscous damping or complex damping. Wang et al. [34]. presented the formulas of energy dissipation in per unit volume of concrete-filled steel tube and reinforced concrete and investigated the stress-dependent damping of frame structures made of different materials. Kume et al. [35] used the damping-stress equation proposed by Lazan [33] and calculated the material damping of a cantilever beam based on the stress distribution without damping. The calculated damping values were found to be in agreement with the experimental values. Gounaris and Anifantis [36] and Gounaris et al. [37] calculated the dynamic responses of cantilever beams using stress-dependent damping and the finite element band method. Mei et al. [38] investigated the effects of the stress amplitude, loading frequency, and stress level on the material damping of concrete. Su et al. [39] performed a seismic analysis of bridges using stress-dependent damping. The results showed that nonlinear damping had a substantial influence on the dynamic behavior of the structure. However, this method has not been used to determine the damping of bridges under vehicle vibration.

In this paper, we propose stress-dependent damping to be used for the analysis of vehicle-bridge coupling vibrations. The dynamic response of bridges and the stress magnitude of the bridge elements under different vehicle speeds conditions were obtained. Subsequently, the stress-dependent damping of bridges was established by using equations of stress related energy dissipation per unit volume. The vehicle-bridge coupling vibration response of a corrugated steel-web bridge was calculated for different vehicle load and speed conditions with constant damping ratio (5%) and stress-dependent damping ratio. The calculated and measured values were compared to validate the proposed model and demonstrated the advantages of using the stress-dependent damping ratio.

2 Vehicle-bridge interaction model

2.1 Vehicle model

Vehicles on a bridge can be simplified as a car body, suspension device, axles, and tires. The primary vehicle's vibrations include vertical vibration, longitudinal and transverse oscillation of the car body, and vertical vibration and transverse oscillation of the wheel set. The schematic diagram of the three-axle vehicle model used in this study is shown in Fig. 1. Table 1 shows the relevant parameters of the tri-axle vehicle.

2.2 Vehicle motion equation

1) Motion equation of the car body

The motion equation describes the vertical vibration, nodding, and rolling of the car body as follows:

$$\begin{aligned} &M_{\mathrm{l}i}\ddot{Z}_{\mathrm{l}i}+\sum_{j=1}^{NW(l,i)}\sum_{k=1}^{2}\left(Z_{\mathrm{l}i}-Z_{\mathrm{l}ij}+\eta_{\mathrm{l}ij}f_{\mathrm{l}ij}\varphi_{\mathrm{l}i}-0.5\eta_k b_{\mathrm{l}ij}\theta_{\mathrm{l}i}+0.5\eta_k b_{\mathrm{l}ij}\theta_{\mathrm{l}ij}\right)k_{\mathrm{sl}jj}\\ &+\sum_{j=1}^{NW(l,i)}\sum_{k=1}^{2}\left(\dot{Z}_{\mathrm{l}i}-\dot{Z}_{\mathrm{l}ij}+\eta_{\mathrm{l}ij}f_{\mathrm{l}ij}\dot{\varphi}_{\mathrm{l}i}-0.5\eta_k b_{\mathrm{l}ij}\dot{\theta}_{\mathrm{l}i}+0.5\eta_k b_{\mathrm{l}ij}\dot{\theta}_{\mathrm{l}ij}\right)c_{\mathrm{sl}jj}=0, \end{aligned} \tag{5}$$

$$\begin{aligned} &J_{q_{\mathrm{l}i}}\ddot{\varphi}_{\mathrm{l}i}+\sum_{j=1}^{NW(l,i)}\sum_{k=1}^{2}\eta_{\mathrm{l}ij}f_{\mathrm{l}ij}\left(Z_{\mathrm{l}i}-Z_{\mathrm{l}ij}+\eta_{\mathrm{l}ij}f_{\mathrm{l}ij}\varphi_{\mathrm{l}i}-0.5\eta_k b_{\mathrm{l}ij}\theta_{\mathrm{l}i}+0.5\eta_k b_{\mathrm{l}ij}\theta_{\mathrm{l}ij}\right)k_{\mathrm{sl}ij}\\ &+\sum_{j=1}^{NW(l,i)}\sum_{k=1}^{2}\eta_{\mathrm{l}ij}f_{\mathrm{l}ij}\left(\dot{Z}_{\mathrm{l}i}-\dot{Z}_{\mathrm{l}jj}+\eta_{\mathrm{l}ij}f_{\mathrm{l}ij}\dot{\phi}_{\mathrm{l}i}-0.5\eta_k b_{\mathrm{l}j}\dot{\theta}_{\mathrm{l}i}+0.5\eta_k b_{\mathrm{l}j}\dot{\theta}_{\mathrm{l}ij}\right)_{\mathrm{sl}jj}=0, \end{aligned} \tag{6}$$

$$\begin{aligned} &J_{0i}\ddot{\theta}_{\mathrm{l}i}-0.5\sum_{j=1}^{NW(l,i)}\sum_{k=1}^{2}\eta_k b_{\mathrm{l}ij}\left(Z_{\mathrm{l}i}-Z_{\mathrm{l}ij}+\eta_{\mathrm{l}ij}f_{\mathrm{l}ij}\varphi_{\mathrm{l}i}-0.5\eta_k b_{\mathrm{l}ij}\theta_{\mathrm{l}i}+0.5\eta_k b_{\mathrm{l}ij}\theta_{\mathrm{l}ij}\right)k_{\mathrm{sl}ij}\\ &-0.5\sum_{j=1}^{NW(l,i)}\sum_{k=1}^{2}\eta_k b_{\mathrm{l}ij}\left(\dot{Z}_{\mathrm{l}i}-\dot{Z}_{\mathrm{l}ij}+\eta_{\mathrm{l}ij}f_{\mathrm{l}ij}\dot{\varphi}_{\mathrm{l}i}-0.5\eta_k b_{\mathrm{l}ij}\dot{\theta}_{\mathrm{l}i}+0.5\eta_k b_{\mathrm{l}ij}\dot{\theta}_{\mathrm{l}ij}\right)c_{\mathrm{sl}ij}=0. \end{aligned} \tag{7}$$

2) Motion equation of the wheel set

The motion equations of the wheel set include vertical and transverse vibrations as follows:

$$\begin{aligned} &m_{\mathrm{l}ij}\ddot{Z}_{\mathrm{l}ij}-\sum_{k=1}^{2}\left(Z_{\mathrm{l}i}-Z_{\mathrm{l}ij}+\eta_{\mathrm{l}ij}f_{\mathrm{l}ij}\varphi_{\mathrm{l}i}-0.5\eta_k b_{\mathrm{l}ij}\theta_{\mathrm{l}i}+0.5\eta_k b_{\mathrm{l}ij}\theta_{\mathrm{l}ij}\right)^2 k_{\mathrm{sl}ij}+\sum_{k=1}^{2}\left(Z_{\mathrm{l}ij}-0.5\eta_k a_{\mathrm{l}ij}\theta_{\mathrm{l}ij}-Z_{\mathrm{l}ijk}\right)k_{\mathrm{tl}ij}\\ &-\sum_{k=1}^{2}\left(\dot{Z}_{\mathrm{l}i}-\dot{Z}_{\mathrm{l}ij}+\eta_{\mathrm{l}ij}f_{\mathrm{l}ij}\dot{\varphi}_{\mathrm{l}i}-0.5\eta_k b_{\mathrm{l}ij}\dot{\theta}_{\mathrm{l}i}+0.5\eta_k b_{\mathrm{l}ij}\dot{\theta}_{\mathrm{l}ij}\right)^2 c_{\mathrm{sl}ij}+\sum_{k=1}^{2}\left(\dot{Z}_{\mathrm{l}ij}-0.5\eta_k a_{\mathrm{l}ij}\dot{\theta}_{\mathrm{l}ij}-\dot{Z}_{\mathrm{l}ijk}\right)c_{\mathrm{tl}ij}=0, \end{aligned} \tag{8}$$

$$J_{\theta ij}\ddot{\theta}_{lij}+0.5\sum_{k=1}^{2}\eta_k b_{lij}\left(Z_{li}-Z_{ljj}+\eta_{lij}f_{lij}\varphi_{li}-0.5\eta_k b_{lij}\theta_{li}+0.5\eta_k b_{lij}\theta_{lij}\right)k_{slij}-0.5\sum_{k=1}^{2}\eta_k a_{lij}\left(Z_{lij}-0.5\eta_k a_{lij}\theta_{lij}-Z_{ljjk}\right)k_{tljj}$$
$$+0.5\sum_{k=1}^{2}\eta_k b_{lij}\left(\dot{Z}_{li}-\dot{Z}_{lij}+\eta_{lij}f_{lij}\dot{\varphi}_{li}-0.5\eta_k b_{lij}\dot{\theta}_{li}+0.5\eta_k b_{lij}\dot{\theta}_{lj}\right)c_{slij}-0.5\sum_{k=1}^{2}\eta_k a_{lij}\left(\dot{Z}_{lij}-0.5\eta_k a_{lj}\dot{\theta}_{lij}-\dot{Z}_{ljjk}\right)c_{tlj}=0. \quad (9)$$

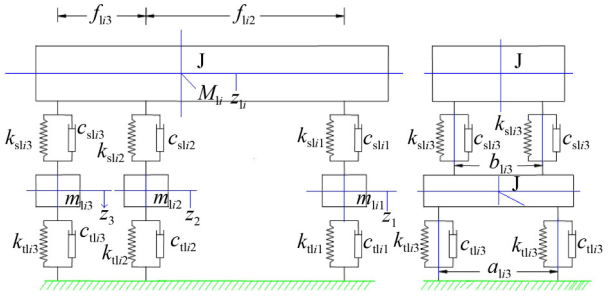

Fig. 1 Three-axle vehicle model.

Table 1 Parameters of the three-axle vehicles

parameter	value
Z_{li}: height of the car body at mass center (m)	1.173
f_{li2}: wheelbase: axle one to axle two (m)	3.6
f_{li3}: wheelbase: axle two to axle three (m)	5
a_{li3}: wheelbase: one axle (m)	1.8
M_{li}: sprung mass (kg)	28500
m_{li1}: unsprung mass: one axis (kg)	550
m_{li2}: unsprung mass: two axes (kg)	550
m_{li3}: unsprung mass: Three axes (kg)	550
k_{sli1}: spring stiffness: one axis (N·mm^{-1})	900
k_{sli2}: spring stiffness: two axes (N·mm^{-1})	2500
k_{sli3}: spring stiffness: three axes (N·mm^{-1})	2500
$K_{tli1\text{-}3}$: tire stiffness (N·mm^{-1})	1300
c_{sli1}: damping: one-axis absorber (kN·m^{-1}·s)	50
c_{sli2}: damping: two-axis absorber (kN·m^{-1}·s)	30
c_{sli3}: damping: two-axis absorber (kN·m^{-1}·s)	30
$c_{tli1\text{-}3}$: damping: tire (kN·m^{-1}·s)	50

Therefore, for the selected tri-axle vehicle, there are nine equations in total, including their equations for the car body and six equations for the wheel set.

2.3 Equation of the vehicle-bridge interaction

A finite element program was utilized to model the bridge and obtain the modal vibration. The modal equations of the different orders of the vibration mode were obtained by discriminating the bridge structures. Thus, the modal equation of an arbitrary order of the vibration mode is expressed as follows:

$$\ddot{x}_n+2\xi_n\omega_n\dot{x}_n+\omega_n^2x_n=F_n, \quad (10)$$

where ξ_n and ω_n are the damping ratio and frequency, respectively, for the nth order vibration mode. The transformation mentioned above is used to express the vibration of the bridge structures with many degrees of freedom (DOFs) using generalized coordinates and the corresponding vibration mode. F_n refers to the force vector transmitted from the vehicle to the bridge by the wheel set.

This study uses the mode superposition method to establish the equilibrium equation of the vehicle-bridge interaction, and uses the Newmark–β method to calculate the dynamic response of the bridge.

A box girder is used as an example, and the dimensions are shown in Fig. 2. The bridge is a pre-stressed simply-supported box girder bridge with corrugated steel webs, with a length of 49.92 m. The strength grade of the cast concrete is C50. The grade of steel material is Q345 high quality steel. The width of the horizontal panel is 430 mm.

A finite element model of the box girder is established in the finite element analysis program Midas. The concrete roof and floor are solid units. The model is shown in Fig. 3.

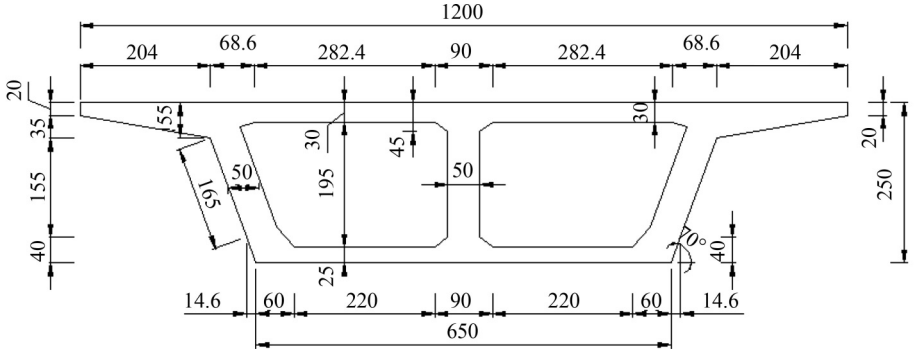

Fig. 2 Sectional dimensions of the box girder with corrugated steel webs (cm).

The vehicle is a tri-axle truck with a total weight of 325 kN, a front axle weight of 65 kN, a central axle weight of 130 kN, a rear axle suspension spring stiffness of 500 kN·m^{-1}, a front axle suspension spring damping of 10 kN·m^{-1}·s, a rear axle suspension spring damping of 2300 kN·m^{-1}·s, and a tire damping of 16 kN·m^{-1}·s.

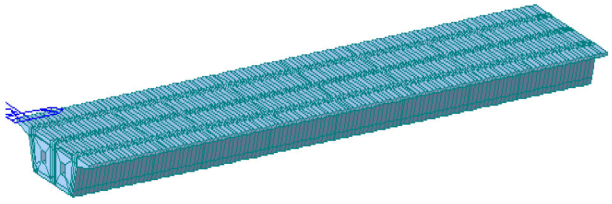

Fig. 3 Model of the box girder with corrugated steel webs.

3 Calculation of stress-dependent damping in the vehicle-bridge system

We define the material dissipation factor as the ratio of the energy dissipation in one vibration cycle to the maximum strain energy as follows:

$$\eta = \frac{2\Delta U}{\pi U}, \quad U = \frac{1}{2}kX^2, \tag{11}$$

where X is the maximum strain.

Assuming a single degree of freedom system response, the energy dissipation in one vibration cycle is:

$$\Delta U = \oint c_e \dot{x} \mathrm{d}x = \int_0^{\frac{2\pi}{\theta}} c_e X^2 \theta^2 \cos^2 \theta t \mathrm{d}t = \pi c_e \theta X^2. \tag{12}$$

We combine Eqs. (11) and (12) to obtain:

$$c_e = \frac{\eta k}{\theta}. \tag{13}$$

In viscous damping, the following applies: $\xi = \frac{c_e}{c_r} = \frac{c_e}{2m\omega}$, then $c_e = 2\xi m\omega$. This equation is substituted into Eq. (13) to obtain:

$$\eta = 2\xi \frac{\theta}{\omega}. \tag{14}$$

Equation (14) describes the relationship between the dissipation factor and the viscous damping ratio. In Eq. (14), it is observed that the conversion of the dissipation factor and viscous damping ratio is significantly influenced by the excitation frequency and natural frequency of vibration. Since vehicle excitations result in a wide frequency spectrum, we assume that the excitation frequency is equal to the natural frequency of vibration, i.e., $\eta = 2\xi$.

Midas Civil is used to model the changes in the stress as the vehicle travels over the bridge. In the analysis process, the basic damping ratio is defined as the damping ratio of the bridge structure tested under environmental excitation, including material damping, auxiliary damping, and adherence damping. In addition, the stress-dependent damping is also considered. The stress-dependent damping is determined using the steps outlined in Fig. 4. The ΔU_1 of steel is related to Wang et al. [34], and the ΔU_2 of concrete is related to Mei et al. [38].

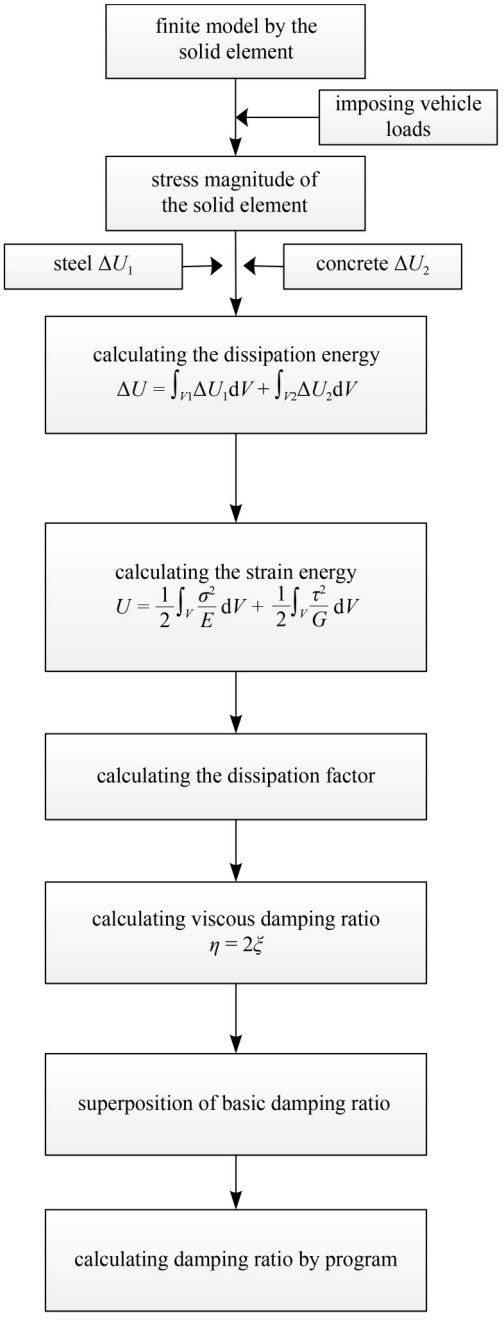

Fig. 4 Calculation steps to determine the stress-related dissipation factors.

4 Results and discussion

4.1 Validation of model performance

We established a finite element model of a concrete box girder using Midas Civil and validated the performance of the proposed program. The vehicle was modeled by moving a triangular load, and the vehicle speed was 60 km/h. The comparison of the mid-span deflections of the bridge obtained from the finite element model and program is shown in Fig. 5.

The average deflection values obtained from the program are generally well aligned with the results obtained by the finite model. However, distinct fluctuations are observed in the results obtained from the program. The primary reason is the difference between the finite model and the program. For example, the finite model does not consider the vibration of the vehicle and the vehicle parameters. In addition, the roughness is not modeled in the finite model.

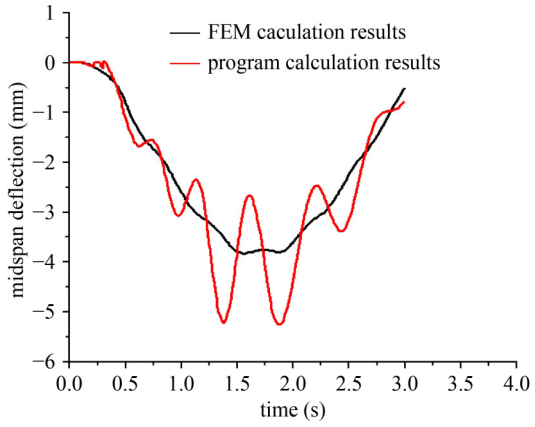

Fig. 5 The deflections in the mid-span of the bridge obtained from the finite element model and proposed program.

4.2 Stress-dependent damping ratio in the vehicle-bridge coupled vibration

The time-history curves of the stress exerted on the bridge when two vehicles with a load of 325 kN each traveled at 30, 60, and 90 km/h and the stress-related damping ratio were obtained. Table 2 shows the calculated stress-dependent damping ratio.

The stress-dependent damping ratio shows an increase with the increasing speed of the vehicles. Under environmental excitation, the bridge has an inherent damping ratio. The measured damping ratio of bridges obtained by Li et al. [16] indicated that the damping ratio of simply-supported girder bridges under environmental excitation is generally less than 3.5%. In the absence of measured data, the basic damping ratio of the bridge is defined as 3% in this study. The calculated damping ratios of the bridge as the two vehicles with a load of 325 kN traveling over the bridge at a speed of 30, 60, and 90 km/h are 3.656%, 3.658%, and 3.671%, respectively.

Table 2 Stress-related damping ratios at different speeds

speed (km/h)	stress-related loss factor (%)	stress-dependent damping ratio (%)
30	1.312	0.656
60	1.316	0.658
90	1.342	0.671

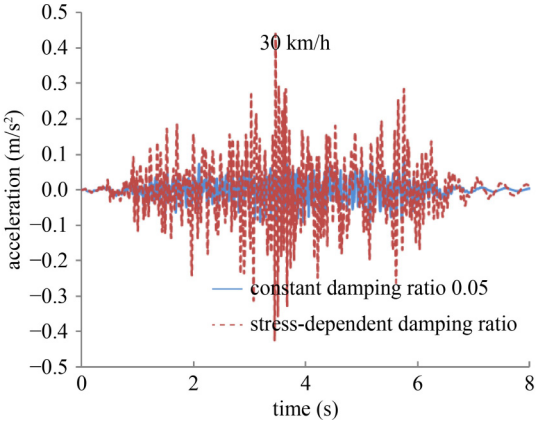

Fig. 6 Midspan acceleration of the bridge for vehicles traveling at 30 km/h.

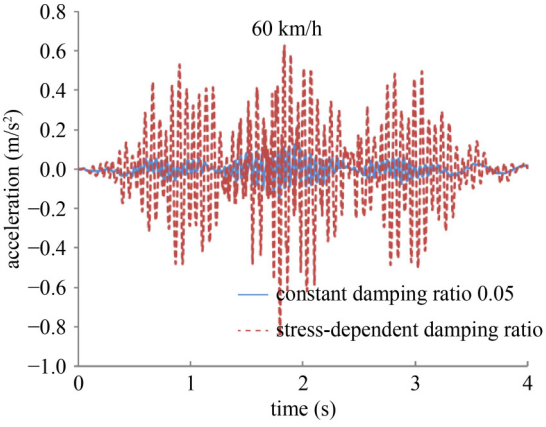

Fig. 7 Midspan acceleration of the bridge for vehicles traveling at 60 km/h.

4.3 Vehicle-bridge coupling vibration with stress-dependent damping

The constant damping ratio (damping ratio = 0.05) and the stress-dependent damping ratio were used to calculate the acceleration response of the mid-span of the bridge for two vehicles with a total weight of 325 kN traveling over the bridge at a speed of 30, 60, and 90. The calculation results are shown in Figs. 6, 7, and 8, respectively.

The results show that the peak acceleration calculated using the constant damping ratio (0.05) is smaller than that calculated using the stress-dependent damping ratio. At the three speeds, the accelerations of the bridge

calculated using the constant damping ratio are 18.9%, 21.3%, and 14.5%, respectively, of the values calculated using the stress-dependent damping ratio. The damping ratio has a significant impact on the acceleration response. High acceleration will exacerbate the deterioration of the bridge structure and affect the driving comfort. Therefore, the stress-dependent damping ratio should be considered by researchers.

Overloading has a severe impact on the safety of bridges. To analyze the influence of overloading on vehicle-bridge coupling vibration, the dynamic response of a vehicle traveling at a speed of 60 km/h at 325 (nominal load) and 650 kN (double the nominal load) load condition was calculated. The time-history curves of the acceleration and deflection at the mid-span of the bridge are shown in Figs. 9 and 10, respectively. The calculated stress-related damping ratio of 650 kN load condition is 0.672%.

The results show that the peak acceleration of the midspan node increased from 126 to 686 mm/s^2 when the vehicle nominal load was doubled, but the stress-dependent damping ratio had increased by only 2.1%. Although increased damping is beneficial to the reduction of the dynamic response, the amplitude of damping increase is limited, and the amplitude of dynamic response increase caused by overloading is large. Overloading increases not only the deflection of the bridge but also impacts the dynamic response. The relative increase in the bridge acceleration is significantly larger than the relative increase in deflection.

4.4 Vehicle-girder bridge vibration with stress-dependent damping

The Sandaohe Middle Bridge located in Qinghai, China, was selected as a case study. The vehicle-bridge coupling vibration response under stress-dependent damping was calculated, and the calculated value was compared with the measured value.

The bridge is a pre-stressed simply-supported box girder bridge with corrugated steel webs, with a length of 49.92 m. Figures 11 and 12 show the structure of the box girder.

The height of the box girder is 250 cm, and the top and bottom edges have lengths of 1200 and 650 cm, respectively. The strength grade of the cast concrete is C50. The vertical sloped angle of the corrugated steel webs is 70°, and the thickness of the corrugated steel webs is 12 mm. The width of the horizontal panel is 430 mm, with a folding angle of 31° and a wave height of 220 mm. Figure 13 shows the schematic diagram of the bridge.

The bridge was tested for accessibility after it was built. During the actual test, vehicles' test speeds were limited to 10 and 20 km/h to avoid damage to the new bridge.

We used the calculation steps shown in Fig. 4 to determine the stress-related dissipation factors and calculated the stress-related damping. The speed parameters were set as 10, 20 and 30 km/h to more genuinely reflect the actual dynamic performance of the bridge. The results are shown in Table 3.

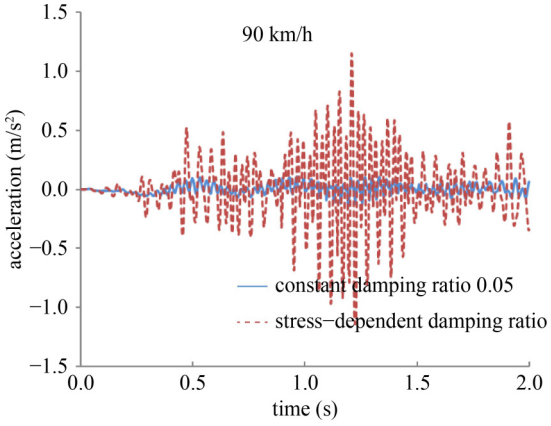

Fig. 8 Midspan acceleration of the bridge for vehicles traveling at 90 km/h.

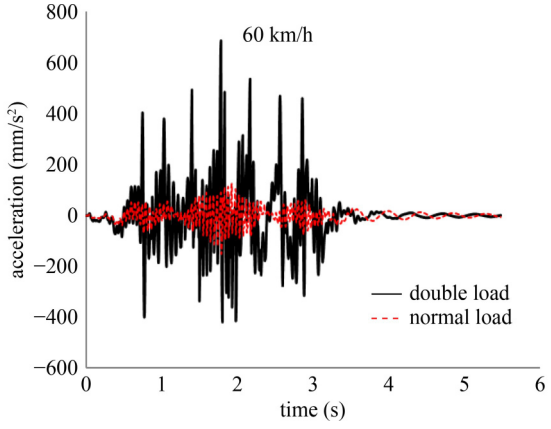

Fig. 9 Midspan acceleration of the bridge for vehicles traveling at 60 km/h.

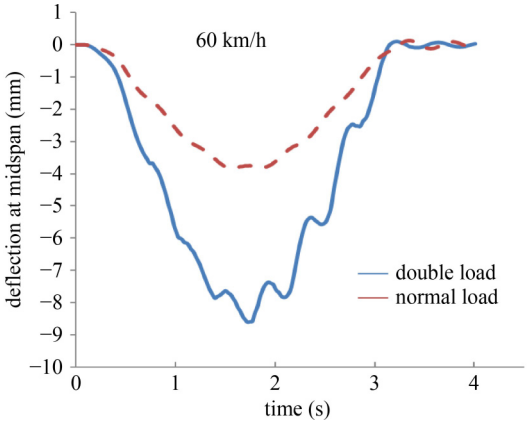

Fig. 10 Midspan deflection of the bridge for vehicles traveling at 60 km/h.

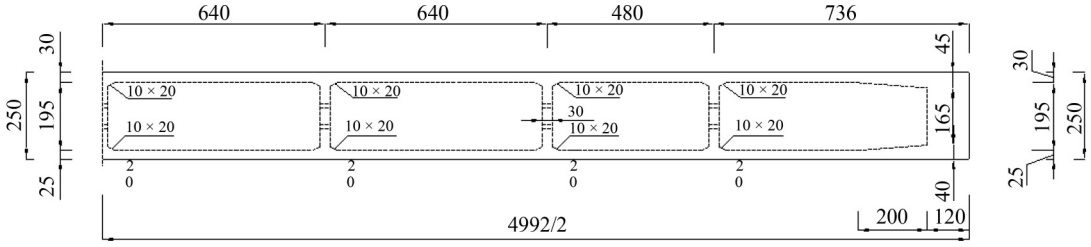

Fig. 11 Profile of the box girder with corrugated steel webs (cm).

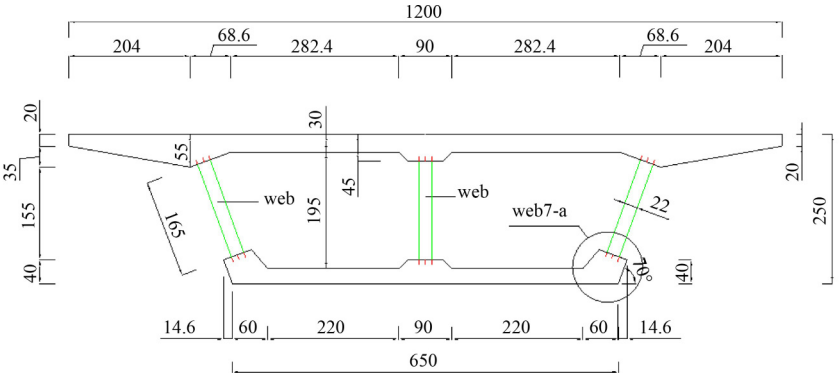

Fig. 12 Sectional dimension of the box girder (cm).

Fig. 13 Schematic diagram of the bridge.

Table 3 Stress-related damping ratios at different speeds

speed (km/h)	stress-dependent dissipation factor (%)	stress-dependent damping ratio (%)
10	1.488	0.744
20	1.480	0.740
30	1.480	0.740

The measured basic damping ratio under environmental excitation is 0.267%, and the damping ratio at different speeds (10, 20, and 30 km/h) is 1.011%, 1.007%, and 1.007%, respectively. The acceleration responses using the constant damping ratio (5%) and the stress-dependent damping ratio and the measured data are shown in Figs. 14 and 15.

The results demonstrate that the stress-dependent damping ratio is superior to the constant damping ratio to calculate the acceleration response of bridges. Both the trend and the peak value of the former are in better agreement with the data measured than that of the latter. The acceleration response is lower when the constant damping ratio is used, which is unfavorable for design applications. However, the stress-dependent damping ratio considers both the basic damping ratio (environmental excitation) and the added damping ratio (forced vibration). The results indicate that the differences between the calculated peak values and the measured peaks value are 7.6% and 5.3% for vehicles traveling at a speed of 10 and 20 km/h, respectively.

5 Conclusions and perspectives

This paper proposed the use of stress-dependent damping to determine vehicle-bridge coupling vibrations. A calculation program was compiled and validated by the finite model. A calculation method for the stress-dependent damping ratio was proposed. A bridge was used as a case study to validate the proposed model and calculate the stress-dependent damping. The vibration responses for stress-dependent damping and constant damping were compared. The following conclusions were then drawn.

1) A calculation method for determining the stress-

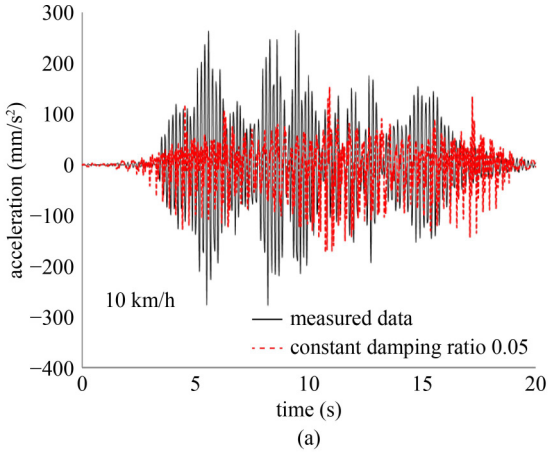

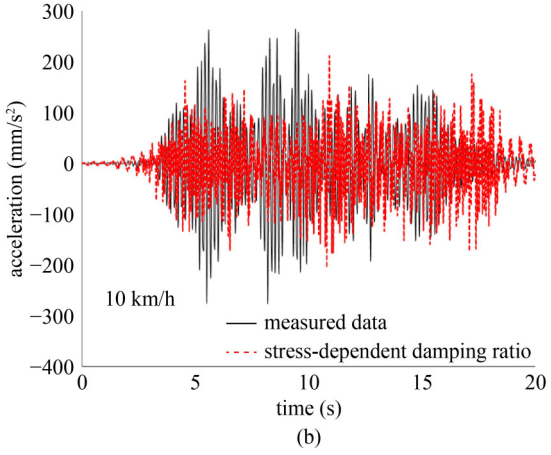

Fig. 14 Acceleration response at the midspan of the bridge for vehicles traveling at 10 km/h. (a) Comparison of the measured data and calculated values (constant damping ratio); (b) comparison of the measured data and calculated values (stress-dependent damping ratio).

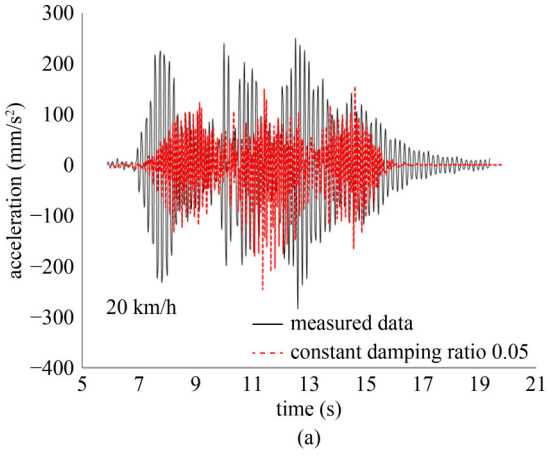

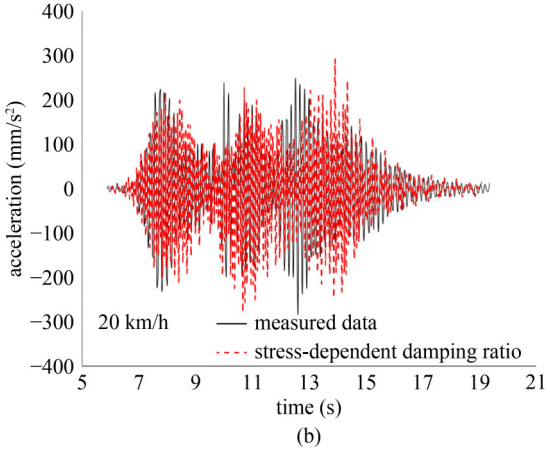

Fig. 15 Acceleration response at the midspan of the bridge for vehicles traveling at 20 km/h. (a) Comparison of the measured data and calculated values (constant damping ratio); (b) comparison of the measured data and calculated values (stress-dependent damping ratio).

dependent damping ratio of a bridge was developed. A model of a simply-supported box girder was established, and the stress of an actual bridge at different vehicle speeds was determined using the stress-dependent damping ratio and a constant damping ratio of 0.05. The coupling vibration response of the vehicle-bridge system was analyzed. The stress value was compared at different vehicle speeds and loads. The acceleration response was determined to be lower when the constant damping ratio of 0.05 was used than the stress-dependent damping ratio.

2) The dynamic response of the bridge at twice the nominal vehicle load was then assessed. The peak acceleration of the mid-span node increased from 126 mm/s^2 to 686 mm/s^2, whereas the stress-related damping ratio of the bridge increased only by 2.1%. Although the increase in damping reduced the dynamic response, the increase in the amplitude was relatively small, while the amplitude of dynamic response increase caused by overloading was determined to be large.

3) The stress-related damping ratio of a composite bridge with corrugated steel webs was calculated. The acceleration response calculated using the stress-dependent damping ratio was closer to the measured acceleration response than when the constant damping ratio (0.05) was used. In practical applications it is challenging to determine the constant damping ratio, and the uncertainty is significant. However, the use of the stress-dependent damping ratio addresses this problem.

This study acknowledges the following limitations.

1) We assumed that the excitation frequency was equal to the natural frequency of vibration to describe the relationship between the dissipation factor and the viscous damping ratio. In future research, different excitation frequencies shall be considered.

2) Actual measurements are needed to determine the basic damping ratio; thus, it is necessary to expand the application's scope.

Acknowledgements This work was supported by the Open Project of National Engineering Laboratory of Bridge Structure Safety Technology of China (No. 2020-GJKFKT-7), the Fundamental Research Funds for Central Research Institutes and Public Service Special Operations of China (No. 2021-9083a), the Key-Area Research and Development Program of

Guangdong Province of China (No. 2019B111106002) and the Fundamental Research Funds for Central Research Institutes and Public Service Special Operations of China (No. 2021-9015b).

References

1. Paultre P, Chaallal O, Proulx J. Bridge dynamics and dynamic amplification factors—A review of analytical and experimental findings. Canadian Journal of Civil Engineering, 1992, 19(2): 260−278
2. Khan E, Lobo J A, Linzell D G. Live load distribution and dynamic amplification on a curved prestressed concrete transit rail bridge. Journal of Bridge Engineering, 2018, 23(6): 04018029
3. Broquet C, Bailey S F, Fafard M, Brühwiler E. Dynamic behavior of deck slabs of concrete road bridges. Journal of Bridge Engineering, 2004, 9(2): 137−146
4. Deng L, Yu Y, Zou Q, Cai C S. State-of-the-art review of dynamic impact factors of highway bridges. Journal of Bridge Engineering, 2015, 20(5): 04014080
5. Yang Y B, Wang Z L, Shi K, Xu H, Yang J P. Adaptive amplifier for a test vehicle moving over bridges: Theoretical study. International Journal of Structural Stability and Dynamics, 2021, 21(3): 2150042
6. Abdel Raheem S E. Dynamic characteristics of hybrid tower of cable-stayed bridges. Steel and Composite Structures, 2014, 17(6): 803−824
7. Mashhadi J, Saffari H. Effects of damping ratio on dynamic increase factor in progressive collapse. Steel and Composite Structures, 2016, 22(3): 677−690
8. Zhang H D, Wang J, Zhang X, Liu G. Effects of viscous damping models on a single-layer latticed dome during earthquakes. Structural Engineering and Mechanics, 2017, 62(4): 455−464
9. Fujino Y, Kimura K, Tanaka H. Wind Resistant Design of Bridges in Japan: Developments and Practices. Berlin: Springer Science & Business Media, 2012
10. Barker R M, Puckett J A. Design of Highway Bridges: An LRFD Approach. New Jersey: John Wiley & Sons, 2013
11. Alipour A, Shafei B, Shinozuka M. Performance evaluation of deteriorating highway bridges located in high seismic areas. Journal of Bridge Engineering, 2011, 16(5): 597−611
12. Code P. Eurocode 8: Design of Structures for Earthquake Resistance. Brussels: European Committee for Standardization, 2001
13. Caltrans S D C. Caltrans Seismic Design Criteria. Version 1.6. Sacramento, CA: California Department of Transportation, 2010
14. Green R. Dynamic response of bridge superstructures-Ontario observations. In: Proceeding of a Symposium of Dynamic Behavior of Bridges at the Transport and Road Research Laboratory. Crowthorne: Transport and Road Research Laboratory (TRRL), 1977
15. Billing J R. Dynamic loading and testing of bridges in Ontario. Canadian Journal of Civil Engineering, 1984, 11(4): 833−843
16. Li P F, Wang Y F, Liu B D, Su L. Damping properties of highway bridges in China. Journal of Bridge Engineering, 2014, 19(5): 04014005
17. Casas J R. Full-scale dynamic testing of the Alamillo cable-stayed bridge in Sevilla (Spain). Earthquake Engineering & Structural Dynamics, 1995, 24(1): 35−51
18. Myrvoll F, Kaynia A M, Hjorth-Hansen E, Strømmen E. Full-scale dynamic performance testing of the bridge structure and the special cable friction dampers on the cable-stayed Uddevalla bridge. In: Proceeding of 20th IMAC Conference on Structural Dynamics, Los Angeles: SPIE Press, 2002
19. Magalhães F, Cunha Á, Caetano E, Brincker R. Damping estimation using free decays and ambient vibration tests. Mechanical Systems and Signal Processing, 2010, 24(5): 1274−1290
20. Rebelo C, Simões da Silva L, Rigueiro C, Pircher M. Dynamic behavior of twin single-span ballasted railway viaducts—Field measurements and modal identification. Engineering Structures, 2008, 30(9): 2460−2469
21. Ülker-Kaustell M, Karoumi R. Application of the continuous wavelet transform on the free vibrations of a steel–concrete composite railway bridge. Engineering Structures, 2011, 33(3): 911−919
22. Ülker-Kaustell M, Karoumi R. Influence of nonlinear stiffness and damping on the train-bridge resonance of a simply supported railway bridge. Engineering Structures, 2012, 41: 350−355
23. Hart G C, Vasudevan R. Earthquake design of buildings: Damping. Journal of the Structural Division, 1975, 101(1): 11−30
24. Charney F A. Unintended consequences of modeling damping in structures. Journal of Structural Engineering, 2008, 134(4): 581−592
25. Eyre R, Tilly G P. Damping measurements on steel and composite bridges. In: Proceeding of a Symposium on Dynamic Behavior of Bridges at the Transport and Road Research Laboratory. Crowthorne: Transport and Road Research Laboratory (TRRL), 1977
26. Tilly G P. Damping of highway bridges: A review. In: Proceeding of a Symposium on Dynamic Behavior of Bridges at the Transport and Road Research Laboratory. Crowthorne: Transport and Road Research Laboratory (TRRL), 1977
27. Green M F, Cebon D. Modal testing of two highway bridges. In: Proceeding of 11th International Modal Analysis Conference. Kissimme (FL): Society for Experimental Mechanics, 1993
28. Hou J L, Xu W B, Chen Y J, Zhang K, Sun H, Li Y. Typical diseases of a long-span concrete-filled steel tubular arch bridge and their effects on vehicle-induced dynamic response. Frontiers of Structural and Civil Engineering, 2020, 14(4): 867−887
29. Sun Z. Moving-inertial-loads-induced dynamic instability for slender beams considering parametric resonances. Journal of Vibration and Acoustics, 2016, 138(1): 011014
30. Jin Z, Huang B, Pei S, Zhang Y. Energy-based additional damping on bridges to account for vehicle-bridge interaction. Engineering Structures, 2021, 229: 111637
31. Glatz B, Fink J. A redesigned approach to the additional damping method in the dynamic analysis of simply supported railway bridges. Engineering Structures, 2021, 241: 112415
32. Stoura C D, Dimitrakopoulos E G. Additional damping effect on bridges because of vehicle-bridge interaction. Journal of Sound and Vibration, 2020, 476: 115294

33. Lazan B J. Damping of Materials and Members in Structural Mechanics. Oxford: Pergamon Press, 1968
34. Wang Y F, Pan Y H, Wen J, Su L. Material damping evaluation of frames made of different materials. Materials Research Innovations, 2014, 18(sup3): 53−58
35. Kume Y, Hashimoto F, Maeda S. Material damping of cantilever beams. Journal of Sound and Vibration, 1982, 80(1): 1−10
36. Gounaris G D, Anifantis N K. Structural damping determination by finite element approach. Computers & Structures, 1999, 73(1-5): 445−452
37. Gounaris G D, Antonakakis E, Papadopoulos C A. Hysteretic damping of structures vibrating at resonance: An iterative complex eigensolution method based on damping-stress relation. Computers & Structures, 2007, 85(23−24): 1858−1868
38. Mei S Q, Su L, Li P F, Wang Y. Material damping of concrete under cyclic axial compression. Journal of Materials in Civil Engineering, 2018, 30(3): 04017295
39. Su L, Wang Y F, Li P F, Mei S, Guo K. Seismic analysis of bridges based on stress-dependent damping. Structural Engineering and Mechanics, 2017, 62(3): 281−289